Nano Energy 57 (2019) 746–752

Contents lists available at ScienceDirect

Nano Energy

journal homepage: www.elsevier.com/locate/nanoen

Full paper

Metal-organic frameworks derived reverse-encapsulation Co-NC@Mo_2C complex for efficient overall water splitting

Qirui Liang, Huihui Jin, Zhe Wang, Yuli Xiong*, Shuai Yuan, Xianci Zeng, Daping He*, Shichun Mu*

State Key Laboratory of Advanced Technology for Materials Synthesis and Processing, Wuhan University of Technology, Wuhan 430070, China
Hubei Engineering Research Center of RF-Microwave Technology and Application, Wuhan University of Technology, Wuhan 430070, China
Hubei Province Engineering Research Center for Intelligent Micro-Nano Medical Equipment and Key Technology, Wuhan Textile University, Wuhan 430200, China

ARTICLE INFO

Keywords:
Metal-organic frameworks
Electrocatalysis
Molybdenum carbide
Cobalt nanoparticles
Water splitting

ABSTRACT

Developing low-cost, highly active, and stable bifunctional electrocatalysts is a challenging issue in electrochemical water electrolysis. Herein, we develop a simple metal organic frameworks (MOFs) based approach to prepare bifunctional Co-NC@ Mo_2C complex catalysts. Differently from traditional carbon encapsulated functional nanomaterials, herein the carbon-based framework derived carbonitride and Co nanoparticles (Co-NC) are encapsulated with Mo_2C. Benefiting from the unique reverse-encapsulation structure and synergetic effects of Mo_2C and Co-NC, the Co-NC@Mo_2C catalyst shows superior hydrogen evolution reaction (HER) and oxygen evolution reaction (OER) performance. In alkaline media, it affords the current density of 10 mA cm^{-2} at low overpotentials of 99 mV and 347 mV for HER and OER, respectively. Interestingly, due to a reversed encapsulation structure where Co nanoparticles are protected by Mo_2C, it leads to an outstanding HER catalytic activity (a low overpotential of 143 mV) and stability in acidic solutions. Remarkably, when employed as both the cathode and anode for overall water splitting, a low cell voltage of 1.685 V is required to reach the current density of 10 mA cm^{-2} in alkaline media with excellent stability, making the Co-NC@Mo_2C an efficient non noble metal bifunctional electrocatalyst toward water splitting.

1. Introduction

Under the concept of sustainable development, hydrogen energy is attracting more and more attention [1–5], and electrocatalytic water splitting is widely regarded as a promising approach for hydrogen generation. The water splitting involves two half reactions: cathodic hydrogen evolution reaction (HER) and anodic oxygen evolution reaction (OER) [6,7], wherein, the key requirement for successful implementation of these two chemical reactions is highly active and stable electrocatlaysts [8]. To date, most of the commercial catalysts are platinum (Pt)-based electrocatalysts for HER and ruthenium (Ru)/iridium (Ir)-based electrocatalysts for OER, respectively [9–12]. However, their high cost and scarcity limit the wide-scale applications. Additionally, HER and OER electrocatalysts often function well in different media, which result in inferior efficiency of overall water splitting when assembled them in the same electrolyte solutions. Therefore, it is highly desirable to rationally design and synthesize cheap and efficient bifunctional catalysts with long stability for water splitting.

Recently, the design and fabrication of porous carbon with hierarchical structures derived from metal organic frameworks (MOFs) has become a hot topic for their potential applications in energy storage, sensor, catalysis etc [13–26]. For example, ZIF-67 have been used as precursors for Co-NC hybrid through facile pyrolysis. The resultant Co-NC complex shows a high surface area, high graphitization degree, a CoNx moiety and uniform N dopant with a regular shape on the nanoscale [27–30]. When applied as OER catalyst, it exhibits excellent activity, approaching the value of Ru or Ir [31,32]. However, common Co-based catalysts suffer from an inferior HER performance [33,34]. To address this problem, researchers have introduced more heteroatoms into Co-based catalysts, such as Pd [35], Ni [36,37], P [38], leading to the change of surface properties and then the enhancement of electrocatalytic performances [7].

On the other side, molybdenum compounds, such as MoC_2, MoS_2, and MoB, are proved to be alternatives for Pt catalyst due to their low costs and impressive HER catalytic performance [39–41]. Particularly, Mo_2C shows highly effective electrocatalytic properties for HER under pH-universal conditions [23,42–45]. For example, Cui et al. prepared Mo_2C nanoparticles decorated graphitic carbon sheets (Mo_2C/GCSs) as

* Corresponding authors.
E-mail addresses: ylxiong@wtu.edu.cn (Y. Xiong), hedaping@whut.edu.cn (D. He), msc@whut.edu.cn (S. Mu).

https://doi.org/10.1016/j.nanoen.2018.12.060
Received 21 November 2018; Received in revised form 12 December 2018; Accepted 18 December 2018
Available online 21 December 2018

an efficient electrocatalyst for hydrogen generation in which the covalent binding between Mo_2C and carbon supports is regarded to facilitate electron transfer and decrease hydrogen binding energy during the HER process [46]. Lu et al. reported Mo_2C-embedded nitrogen-doped porous carbon nanosheets (Mo_2C@2D-NPCs) with a low overpotential for HER in alkaline solution in which the strong interaction between Mo_2C and NPC reduces the energy barrier for water splitting [47]. Recently, our group also obtained a Mo_2C quantum dot embedded N-doped graphitic carbon layer (Mo_2C QD/NGCL) with outstanding HER catalytic activity and stability at all pH values [48].

In this work, we report a MOF-based approach to prepare Co-NC@Mo_2C complex with integrated advantages of Mo_2C and Co-NC for water splitting. The as-prepared catalyst is Mo_2C coated derivations of carbonitride and Co nanoparticles (NPs), where the coating structure of Mo_2C not only protects the inner layer of Co NPs from electrolyte erosion, but also provides more metal and carbon contact sites. Benefiting from the excellent bifunctional catalytic property, Co-NC@Mo_2C shows outstanding catalytic activities in both HER and OER in an alkaline electrolyte. When employed as electrocatalysts for both anode and cathode in an overall water electrolyzer (1.0 M KOH), a cell voltage of only 1.685 V at 10 mA cm^{-2} and long-term durability (20 h) is achieved, which functioning the Co-NC@Mo_2C as a versatile electrode for efficient overall water splitting.

2. Experimental section

2.1. Materials and reagent

Analytical grade zinc nitrate hexahydrate ($Zn(NO_3)_2{\cdot}6H_2O$), cobalt nitrate hexahydrate ($Co(NO_3)_2{\cdot}6H_2O$), ammonium molybdate tetrahydrate were obtained from Sinopharm Group Chemical Reagent. 2-Methylimidazole was obtained from Aladdin Reagents Ltd. The commercial Pt/C (20%) catalyst was purchased from Johnson Mattey, while both of commercial Mo_2C and commercial IrO_2 catalysts were purchased from Alfa Aesar. All the reagents were analytical grade and used as received. High-purity water was supplied by a Millipore system.

2.2. Synthesis of ZIF-67

186 mg $Co(NO_3)_2{\cdot}6H_2O$ was dissolved in 5 mL methanol solution. Then, the solution was mixed with 5 mL methanol solution containing 205 mg 2-Methylimidazole, and stirred at room temperature for 4 h. After that, the product was collected by centrifugation and washed by methanol for three times and dried at 60 ℃ overnight.

2.3. Synthesis of ZIF-8

182 mg $Zn(NO_3)_2{\cdot}6H_2O$ was dissolved in 5 mL methanol solution. Then, the solution was mixed with 5 mL methanol solution containing 205 mg 2-Methylimidazole, and ultrasound the mixed solution for 20 min. After standing for 12 h, the product was collected by centrifugation and washed by methanol for three times and dried at 60 ℃ overnight.

2.4. Synthesis of Co-NC@Mo_2C

The as prepared ZIF-67 was further ground thoroughly with ammonium molybdate tetrahydrate, then annealed at 700 ℃ for 3 h with a ramp rate of 5 ℃ min^{-1} under a flow of high purity argon gas. The obtained product was Co-NC@Mo_2C.

2.5. Synthesis of NC@Mo_2C

The as prepared ZIF-8 was further ground thoroughly with ammonium molybdate tetrahydrate, then annealed at 700 ℃ for 3 h with a ramp rate of 5 ℃ min^{-1} under a flow of high purity argon gas. The obtained product was NC@Mo_2C.

2.6. Synthesis of Co-NC

The as prepared ZIF-67 was further annealed at 700 ℃ for 3 h with a ramp rate of 5 ℃ min^{-1} under a flow of high purity argon gas. The obtained product was Co-NC.

2.7. Synthesis of NC

The as prepared ZIF-8 was further annealed at 700 ℃ for 3 h with a ramp rate of 5 ℃ min^{-1} under a flow of high purity argon gas. The obtained product was NC.

2.8. Characterization

X-ray diffraction (XRD) patterns were collected on a X-Bruker D8 Advance Ray Diffractometer with Cu Kα radiation (λ = 1.5406 Å). The morphologies of the products were characterized by field-emission scanning electron microscope (FESEM; XL30 ESEM FEG) and transmission electron microscope (TEM; Hitachi, Tokyo, Japan, HITACHI H-8100). The composition of the samples was characterized by energy-dispersive X-ray spectroscopy (EDX) attached to the FESEM. HAADF-STEM image and elemental mapping were collected using a TEM (FEI Titan Them) equipped with EDX spectroscopy. X-ray photoelectron spectrometer (XPS, Thermo Fischer ESCALAB 250Xi) and Inductively Coupled Plasma-Optical Emission Spectra (ICP, Prodigy 7) was used for analysis of the composition of the as-synthesized sample. Raman spectra were collected on a Renishaw Invia Reflex Raman microscope equipped with a 514 nm excitation laser.

2.9. Electrochemical measurements

Firstly, 5.0 mg catalyst powder was dispersed in 500 μL ethanol solvents. Then, the solution was mixed with 10 μL 5 wt% Nafion solution and sonicated for 10 min. Finally, 6 μL catalyst ink was loaded on a glassy carbon electrode (GCE: diameter = 3 mm) at a catalyst loading of about 0.83 mg cm^{-2}.

HER and anodic OER electrochemical measurements were performed on an Autolab-PG302N electrochemical analyzer in a standard 3-electrode with 2-compartment cell. Ag/AgCl (KCl saturated) was used as the reference electrode for the acidic (0.5 M H_2SO_4) electrochemical measurements. Hg/HgO was used as the reference electrode for the alkaline (1.0 M KOH) electrochemical measurements. Graphite plate was used as the counter electrode in above measurements. The reference electrode was corrected with regard to reversible hydrogen electrode (RHE) in all measurements, and the scan rate of obtaining polarization data was kept at 5 mV s^{-1}. Pt wire was used as the working electrode in the high purity hydrogen saturated electrolyte for calibration. With the 5 mV s^{-1} scan rate of current-voltage, the average value of two potentials of zero crossing current is taken as the thermal dynamic potential of H-electrode reaction. The catalyst Co-NC@Mo_2C loaded on GCE was used as both cathode and anode in a two-electrode configuration for overall water splitting. The LSV curves were obtained at a scan rate of 5 mV s^{-1} and chronoamperometry experiments were conducted at applied bias voltage of 1.69 V for 20 h. All polarization curves were IR-corrected. The amount of H_2/O_2 generated in the H-type electrolytic cell was collected by the water drainage method. The water-splitting device uses carbon paper as electrodes (2 × 2 cm) precoated with Co-NC@Mo_2C.

3. Results and discussion

The synthesis procedure for Co-NC@Mo_2C is illustrated in Fig. 1a. ZIF-67 (or ZIF-8) was prepared according to the reference [49]. As shown in Fig. 1b (Fig. S1 and S2), ZIF-67 displays a rhombic

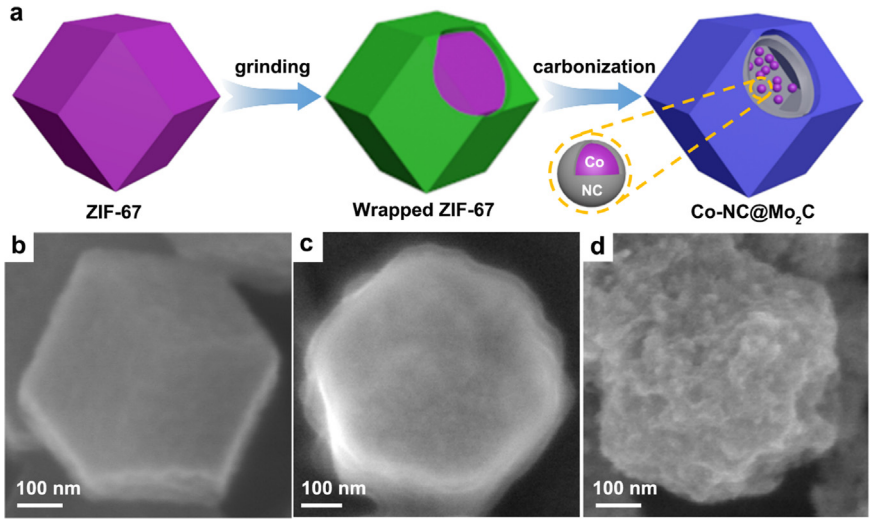

Fig. 1. (a) Diagram of the formation process of Co-NC@Mo_2C. (b–d) FESEM images of the as-prepared ZIF-67, ammonium molybdate tetrahydrate wrapped ZIF-67 and Co-NC@Mo_2C.

dodecahedron structure and a size of around 500 nm with a smooth surface. Then, the same mass of ZIF-67 and ammonium molybdate tetrahydrate was ground together. ZIF-67 was wrapped by ammonium molybdate and the surface becomes rougher (Fig. 1c and Fig. S3) compared to pristine ZIF-67. After carbonized under high purity argon atmosphere, Co ions from ZIF-67 were reduced to form Co NPs, and the organic moiety could form carbonitride surrounding the Co NPs. Meanwhile, ammonium molybdate was converted into Mo_2C with possible chemical reactions as follows [50]:

$$(NH_4)_6{\cdot}Mo_7O_{24}{\cdot}4H_2O = 7MoO_3 + 6NH_3 + 7H_2O \quad (1)$$

$$2MoO_3 + 4C = Mo_2C + 3CO_2 \quad (2)$$

where, firstly, ammonium molybdate is decomposed into ammonia, MoO_3 and water. Then the resulting MoO_3 reacts with the carbon skeleton of ZIF-67 and generates Mo_2C. It can be seen clearly from the SEM images (Fig. 1d and Fig. S4) and TEM images (Fig. 2a and Fig. S5) that Co-NC@Mo_2C still keeps the rhombic dodecahedron structure, although some carbon skeletons collapsed probably due to the water production and consumption of C in the chemical reactions. From the high-resolution TEM (HR-TEM) image (Fig. 2b), its surface shows clear lattice fringes with interplanar distance of 0.149 and 0.228 nm, corresponding to the (110) and (101) crystal planes of the Mo_2C nanoparticles, respectively. It is difficult to see the outline and lattice fringes of Co nanoparticles clearly when Mo_2C wrapped the Co-NC. However, Co nanoparticles with the lattice fringes corresponding to (111) plane can be seen faintly in those collapsed structures, as shown in Fig. S6.

The EDX spectrum (Fig. S7) and elemental mapping (Fig. 2c) reveal the existence of Co and Mo in Co-NC@Mo_2C. Besides, from the distribution of Co and Mo in elemental mapping figures, we can find that the Co element only concentrates in the inner part of carbon frameworks, whereas the Mo element is distributed in the edge, which further

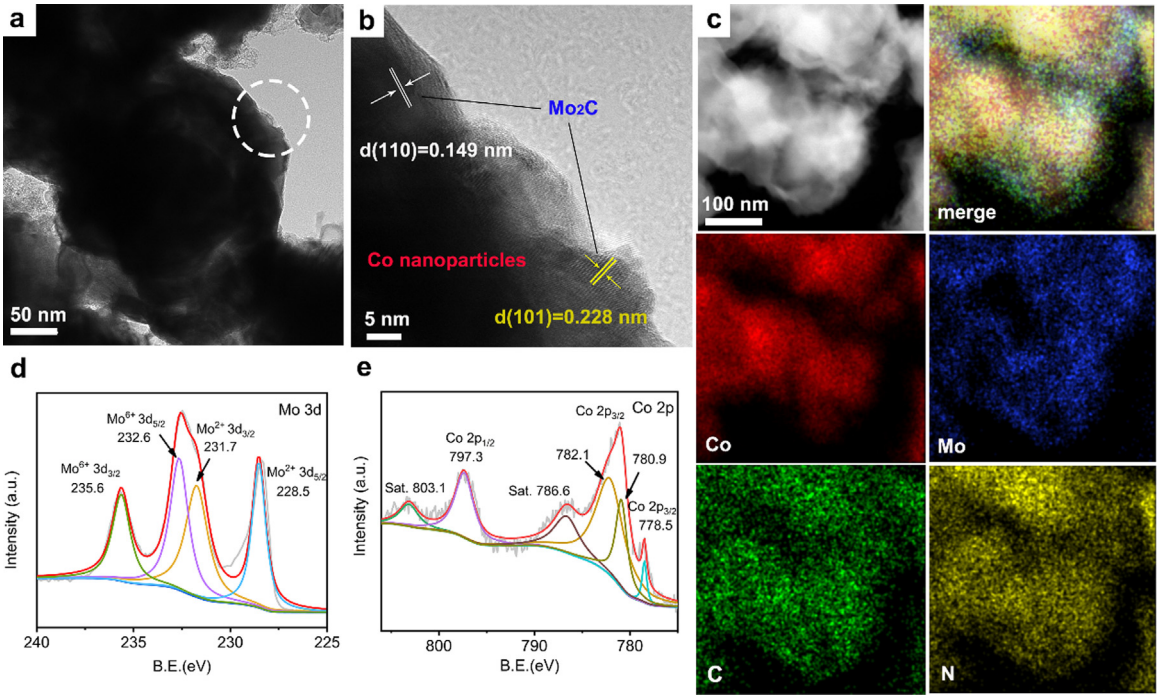

Fig. 2. (a) TEM image, (b) HRTEM image, (c) HAADF-STEM and EDX elemental mapping of Co-NC@Mo_2C. XPS spectra of Co-NC@Mo_2C: (d) Mo 3d. (e) Co 2p.

confirms the encapsulation of Mo_2C on the surface of whole carbon skeleton. In addition, the results of Inductively Coupled Plasma (ICP) test also indicate the existence of Co and Mo element in Co-NC@Mo_2C (Table S1).

In the control experiments, NC@Mo_2C was obtained by the same method except ZIF-67 was replaced by ZIF-8, while the pyrolysis derivations of ZIF-8 and ZIF-67 under high purity argon atmosphere was NC and Co-NC, respectively. The surface of Co-NC (Fig. S8) is very smooth, and ZIF-8 (Fig. S9) shows a similar structure to ZIF-67 and Mo_2C wrapped around carbon framework in NC@Mo_2C (Fig. S10), as a normal encapsulated structure.

From the X-ray diffraction (XRD) results in Fig. S11, NC shows disappearance of all the sharp peaks of the pristine ZIFs. Instead, a new broad peak emerges at $2\theta = 22.6^{\circ}$, due to agraphitic C diffraction, which indicates there are little graphite domains presented in the samples [51]. Compared with NC, another obvious diffraction peak is observed at $2\theta = 44.37^{\circ}$ for Co-NC and $2\theta = 39.49^{\circ}$ for NC@Mo_2C, indexing to (111) plane of Co (JCPDS No. 01-1255) [52] and (101) plane of Mo_2C (JCPDS No. 11-0680) [53], respectively. For Co-NC@Mo_2C, it has one broad peak and two strong diffractions peaks, corresponding to agraphitic C diffraction, Co (111) and Mo_2C (101), respectively. As shown in Fig. S12, Co-NC@Mo_2C possesses the D peak (1582 cm^{-1}) for sp^{2-} hybridized carbon and G peak (1330 cm^{-1}) for lattice defects of a typical carbon material with a low degree of graphitization. Besides, it has additional peaks assignable to the Mo-coupling phases and doped Co-species [23,31].

The X-ray photoelectron spectroscopy (XPS) results of Co-NC@Mo_2C indicate the existence of Co, Mo, C, N, and O elements (Fig. S13a) with the atomic ratio of 6.94%, 13.41%, 19.64%, 28.57%, and 31.45%, respectively (Table S2). The Mo 3d spectrum (Fig. 2d) displays two pairs of peaks (Mo $3d_{5/2}/3d_{3/2}$) at binding energies of 232.6/235.6 and 228.5/231.7 eV, attributed to surface-oxidized MoO_x caused by the exposure to ambient atmosphere [46] and Mo_2C, respectively [47]. The spectrum of Co 2p (Fig. 2e) can be deconvoluted into three major peaks located at 781.3, 778.5 eV for Co $2p_{3/2}$ and 797.3 eV for Co $2p_{1/2}$, respectively. The peak of Co $2p_{3/2}$ in 781.3 eV can be further split into subpeaks of Co^{3+} (780.9 eV) and Co^{2+} (782.1 eV). The peak of Co $2p_{3/2}$ in 778.5 eV indicates the existence of a metallic state of Co. [54–56] Two additional shake up satellite peaks are also observed at binding energy of 803.1 and 786.6 eV, which indicates the oxidized surface species owing to exposure to the atmosphere. [31,57] The deconvoluted C 1s binding energy spectrum can be demonstrated as three peaks, corresponding to C=C/C-C (284.6 eV), C=N (285.4 eV) and C-N (288.7 eV) bonds, respectively (Fig. S13b) [48]. Two peaks of the N 1s spectrum (Fig. S13c) can be ascribed to pyridinic N (397.7 eV) and graphitic N (399 eV), respectively [50], while the pyridinic N is the main nitrogen species in Co-NC@Mo_2C, which is good for the HER because the lone electron pair in the plane of the carbon matrix can elicit electron and active hydrogen [51].

To evaluate the electrocatalytic behavior, samples were investigated by linear sweep voltammograms (LSV) in alkaline solution (Fig. 3a), the overpotentials for Co-NC, NC@Mo_2C, NC and commercial Mo_2C are 340 mV, 173 mV, 545 mV and 238 mV (at the current density of 10 mA cm^{-2}), respectively, while Co-NC@Mo_2C at 700 °C (Fig. S14) displays much better catalytic activity (η @ 10 mA cm^{-2} = 99 mV) than the contrast samples except the commercial Pt/C. As shown in Fig. 3b, the Tafel slope of Co-NC@Mo_2C (65 mV dec^{-1}) is around 4 mV dec^{-1}, lower than the Pt/C (20 wt%) (69 mV dec^{-1}) and much lower than the other catalysts used in this study (demonstrated in Table S3). When Co-NC@Mo_2C was operated for stability test (Fig. 3c), the LSV curves of the 1st and 1000th cycle almost overlap, and the current density has 87.7% retention after 25 h, demonstrating the higher stability of Co-NC@Mo_2C compared with commercial Pt/C (Fig. S15a) in alkaline medium.

Due to the acid corrosion of Co NPs, the HER performance of common carbon-supported Co NPs catalysts is not good under acidic conditions [38,58,59]. However, in such a reversed encapsulation structure, Co NPs are protected by Mo_2C in this work, so Co-NC@Mo_2C still shows an outstanding catalytic activity in 0.5 M H_2SO_4 aqueous solution. As shown in Fig. 3d, although commercial Pt/C still shows the best performance (η@10 mA cm^{-2} = 35 mV). Co-NC@Mo_2C also performs well (η@10 mA cm^{-2} = 143 mV), which is much better than the Co-NC (526 mV), NC@Mo_2C (179 mV), NC (500 mV) and commercial Mo_2C (394 mV) as well as other catalysts reported (Table S4). Meanwhile, it shows a small Tafel slope (60 mV dec^{-1}) (Fig. 3e) and better electrocatalytic stability than commercial Pt/C (Fig. S15b), where the current density has around 81% retention after 25 h and little reduction after 1000th cycles (Fig. 3f). After the durability tests, the XPS spectra (Fig. S16) of Co-NC@Mo_2C were collected, and the strength of peaks for Mo^{2+} corresponding to Mo_2C weaken after HER stability test in acidic solution (Fig. S16b), which indicates Mo_2C in Co-NC@Mo_2C is the main participant in HER and the loss of Mo_2C during the reaction results in the decrease of catalyst performance. Besides, the peaks corresponding to the metallic Co state disappear after stability test(Fig. S16c), showing that a small amount of Co nanoparticles on the surface were consumed during the reaction. Yet, there is only a slight decrease about the elemental atomic ratio of Co and Mo after durability test (Table S5), and the XRD patterns before and after stability test (Fig. S17) shows no obvious change. In addition, the SEM image (Fig. S18) indicates that the sample almost maintains the pristine morphology. These confirm that Co-NC@Mo_2C has a good HER stability in acid media.

The capacitive currents of Co-NC@Mo_2C (Fig. S19a), Co-NC (Fig. S19b) and NC@Mo_2C (Fig. S19c) were measured in a potential range between −0.60 to −0.50 V without faradic processes. The differences in current density variation at the potential of −0.55 V plotted against scan rate were fitted. As seen from Fig. S19d, the capacitance of Co-NC@Mo_2C, Co-NC and NC@Mo_2C is 85.82, 43.80 and 57.74 mF cm^{-2}, respectively, which is consistent with their HER performances.

The OER performance of catalysts in 1.0 M KOH aqueous solution is shown in Fig. 4. In contrast to Co-NC (η@10 mA cm^{-2} = 375 mV), NC@Mo_2C (η@5 mA cm^{-2} = 524 mV) and other reported similar catalysts (Table S6), Co-NC@Mo_2C (η@10 mA cm^{-2} = 347 mV) has a great performance, which is comparable to commercial IrO_2 catalysts (η@10 mA cm^{-2} = 316 mV) (Fig. 4a). The OER performances of NC@Mo_2C and commercial Mo_2C (η@10 mA cm^{-2} = 518 mV) suggest that pristine Mo_2C has little catalytic activity in 1.0 M KOH aqueous solutions, which further proves that the excellent OER activity of Co-NC@Mo_2C is because of the unique structure and synergetic effects of Mo_2C and Co-NC. The Tafel slope (Fig. 4b) of Co-NC@Mo_2C (61 mV dec^{-1}) is much lower than the other catalysts used in this study (demonstrated in Table S3), and around 27 mV dec^{-1} lower than the commercial IrO_2 (88 mV dec^{-1}). When Co-NC@Mo_2C was operated at overpotential of about 350 mV in a 1.0 M KOH aqueous solution, it shows more excellent electrochemical stability compared with commercial IrO_2 (Fig. S20a) with 73% retention after 20 h and 10 mV potential attenuation after 1000th cycles (Fig. 4c).

The point diagram of the Tafel slope and the overpotential/voltage corresponding to 10 mA cm^{-2}/5 mA cm^{-2} of all catalysts are shown in Fig. S21. Co-NC@Mo_2C shows an outstanding HER and OER performances. Thus, we assembled an electrolyzer by using Co-NC@Mo_2C as electrocatalyst in 1.0 M KOH aqueous solutions. LSV curves were collected (Fig. 4d) and obvious H_2 and O_2 bubbles can be observed (inset in Fig. 4d). It delivers a voltage of 1.685 V at 10 mA cm^{-2}, which is only around 67 mV worse than the commercial IrO_2-Pt/C catalyst, comparable to that of the excellent catalyst reported (Table S7). The corresponding Tafel slopes (Fig. 4e) are also consistent with the results of LSV curves. Moreover, as shown in Fig. 4f, the system remains 79.2% catalytic performance at 1.69 V after 20 h and around 18 mV reduction of the current density after 1000th cycles, which is superior to commercial IrO_2-Pt/C catalyst (Fig. S20b).

The amount of H_2/O_2 generated in the H-type electrolytic cell based on Co-NC@Mo_2C catalyst was collected by the water drainage method (Fig. 5a and Fig. S22). Figs. 5b–e (or Figs. 5f–i) reveals the volume of H_2

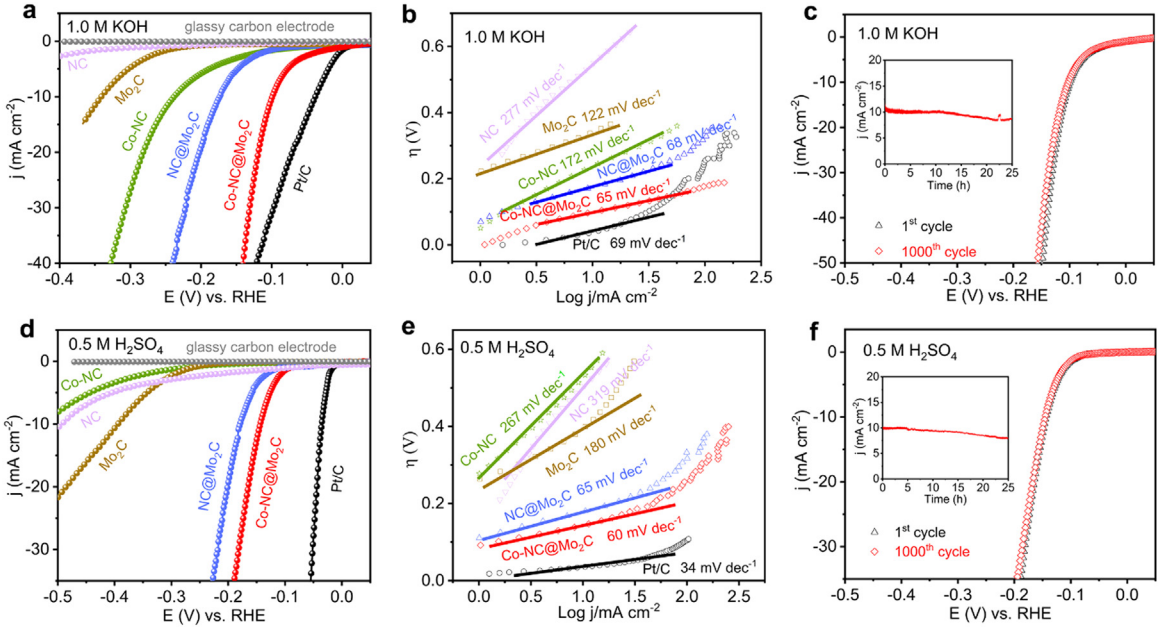

Fig. 3. (a, d) HER polarization curves of Co-NC@Mo_2C and other catalyzers in 1.0 M KOH aqueous solution and 0.5 M H_2SO_4 aqueous solution respectively at a scan rate of 5 mV dec^{-1}. (b, e) Corresponding Tafel curves. (c, f) Time-dependent current density curves for Co-NC@Mo_2C at constant potentials for 25 h and corresponding polarization curves before and after 1000 CV cycles.

(or O_2) generated by the cell. The electrolyte is separated by Nafion membrane (Fig. 5j), and the bubbles can be clearly seen on carbon paper (Figs. 5k and l). The Faradaic efficiency is demonstrated to be close to 100% for overall water splitting with the H_2 to O_2 volume ratio of 2.13:1 (considering the influence of device air tightness), approaching the theoretical value of 2:1 during electrolysis (Fig. 5m). This result manifests that Co-NC@Mo_2C is indeed an efficient and durable electrocatalyst toward water splitting.

4. Conclusion

In summary, we successfully synthesized Co-NC@Mo_2C (Mo_2C coated derivations of carbon nitride and Co NPs). The reversed encapsulation effect of Mo_2C not only protects the normal electrocatalytic reaction of carbon-supported Co NPs, but also provides more metal sites for reaction, and ultimately enhances the catalytic performance of the whole catalyst. Compared with other reported similar catalysts, Co-NC@Mo_2C shows not only excellent HER electrocatalytic performance in acid (η@10 mA cm^{-2} =143 mV in 0.5 M H_2SO_4) and alkaline (η@10 mA cm^{-2} = 99 mV in 1.0 M KOH) solutions, but also great OER

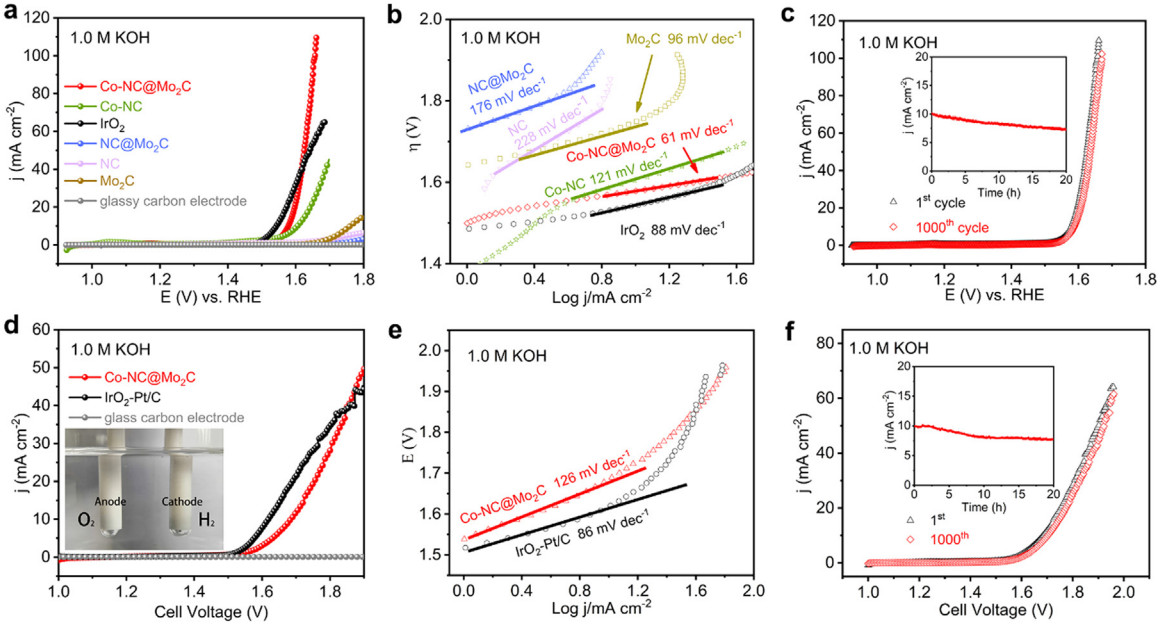

Fig. 4. (a) OER polarization curves of Co-NC@Mo_2C and other catalyzers in 1.0 M KOH aqueous solutions at a scan rate of 5 mV dec^{-1}. (b) Corresponding Tafel curves. (c) Time-dependent current density curves for Co-NC@Mo_2C at constant potentials for 20 h and corresponding polarization curves before and after 1000 CV cycles. (d) LSV curves of overall water splitting in a two-electrode configuration. The inset is the digital photo of H_2 and O_2 bubbles. (e) Corresponding tafel curves. (f) Time-dependent current density curves for Co-NC@Mo_2C at constant potentials for 20 h and corresponding polarization curves before and after 1000 CV cycles.

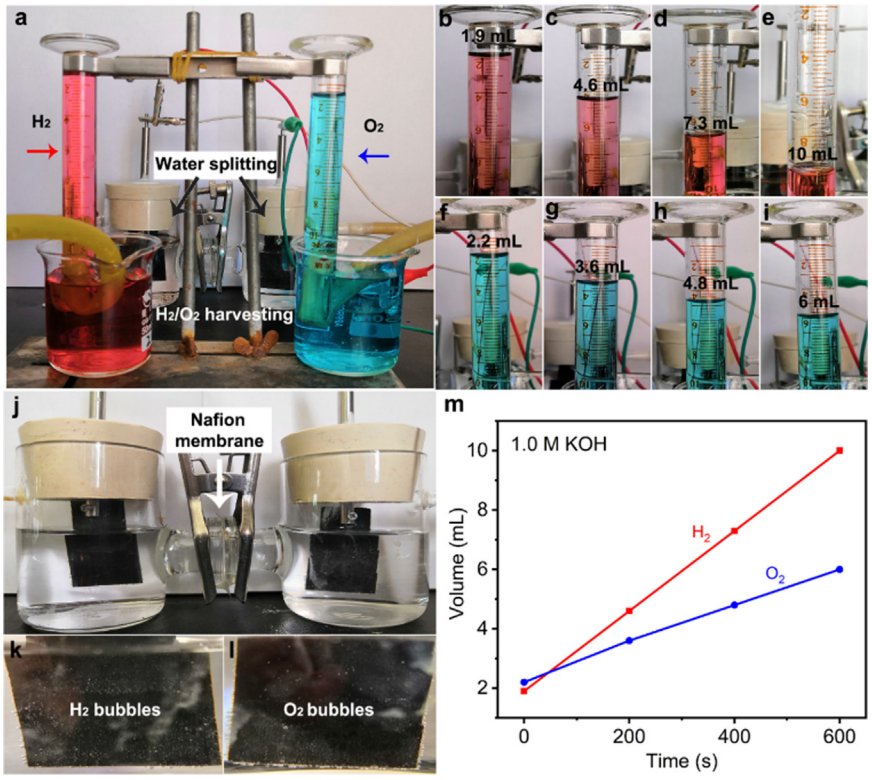

Fig. 5. (a) Gas collection device of water splitting in 1.0 M KOH aqueous solution. (b, c, d, e) Enlarged digital images of the measuring cylinders shown in (a), and levels of hydrogen gas generated at 0, 200, 400, 600 s. (f, g, h, i) Corresponding levels of oxygen gas generated at 0, 200, 400, 600 s. (j) Digital image of the electrolyzed water reaction tank separated by Nafion membrane. (k) Digital image of H_2 bubbles attached to carbon paper. (l) Digital image of O_2 bubbles attached to carbon paper. (m) Amount of H_2/O_2. Time-dependent experimentally measured versus time for Co-NC@Mo_2C in 1.0 M KOH aqueous solution.

electrocatalytic performance in alkaline solutions (η@10 mA cm^{-2} = 347 mV in 1.0 M KOH). This bifunctional catalytic property allows Co-NC@Mo_2C to be used as an outstanding catalyst for efficient water splitting. Our study opens up a new way for the design of MOF derived catalysts to obtain multifunctional catalytic performance.

Acknowledgments

This work was supported by the National Natural Science Foundation of China (51701146, 51672204).

Appendix A. Supporting information

Supplementary data associated with this article can be found in the online version at doi:10.1016/j.nanoen.2018.12.060.

References

[1] Z. Xi, H. Lv, D.P. Erdosy, D. Su, Q. Li, C. Yu, J. Li, S. Sun, Nanoscale 9 (2017) 7745–7749.
[2] J. Yin, Q. Fan, Y. Li, F. Cheng, P. Zhou, P. Xi, S. Sun, J. Am. Chem. Soc. 138 (2016) 14546–14549.
[3] Y. Li, Y. Wang, B. Pattengale, J. Yin, L. An, F. Cheng, Y. Li, J. Huang, P. Xi, Nanoscale 9 (2017) 9230–9237.
[4] S. Rehman, S. Guo, Y. Hou, Adv. Mater. 28 (2016) 3167–3172.
[5] X.L. Tian, L. Wang, P. Deng, Y. Chen, B.Y. Xia, J. Energy Chem. 26 (2017) 1067–1076.
[6] Y. Jiao, Y. Zheng, M. Jaroniec, S.Z. Qiao, Chem. Soc. Rev. 44 (2015) 2060–2086.
[7] Y. Zheng, Y. Jiao, M. Jaroniec, S.Z. Qiao, Angew. Chem. Int. Ed. 54 (2015) 52–65.
[8] Y.F. Xu, M.R. Gao, Y.R. Zheng, J. Jiang, S.H. Yu, Angew. Chem. Int. Ed. 52 (2013) 8546–8550.
[9] M.R. Gao, Y.F. Xu, J. Jiang, Y.R. Zheng, S.H. Yu, J. Am. Chem. Soc. 134 (2012) 2930–2933.
[10] Y.R. Zheng, M.R. Gao, Z.Y. Yu, Q. Gao, H.L. Gao, S.H. Yu, Chem. Sci. 6 (2015) 4594–4598.
[11] J. Zhang, L. Qu, G. Shi, J. Liu, J. Chen, L. Dai, Angew. Chem. Int. Ed. 55 (2016) 2230–2234.
[12] J. Wang, L. Gan, W. Zhang, Y. Peng, H. Yu, Q. Yan, X. Xia, X. Wang, Sci. Adv. 4 (2018) eaap7970.
[13] Y. Hou, Z. Wen, S. Cui, S. Ci, S. Mao, J. Chen, Adv. Funct. Mater. 25 (2015) 872–882.
[14] P. He, X.Y. Yu, X.W. Lou, Angew. Chem. Int. Ed. 56 (2017) 3897–3900.
[15] Z. Li, B.Y. Guan, J. Zhang, X.W. Lou, Joule 1 (2017) 576–587.
[16] B.Y. Guan, X.Y. Yu, H.B. Wu, X.W.D. Lou, Adv. Mater. 29 (2017) 1703614.
[17] Z. Li, M. Shao, L. Zhou, R. Zhang, C. Zhang, M. Wei, D.G. Evans, X. Duan, Adv. Mater. 28 (2016) 2337–2344.
[18] H. Wang, L. Xiang, W. Wei, J. An, J. He, C. Gong, Y. Hou, ACS Appl. Mater. Interfaces 9 (2017) 42102–42110.
[19] L. Yu, J.F. Yang, X.W. Lou, Angew. Chem. Int. Ed. 55 (2016) 13422–13426.
[20] P. Zhang, B.Y. Guan, L. Yu, X.W.D. Lou, Angew. Chem. Int. Ed. 56 (2017) 7141–7145.
[21] H. Jin, H. Zhou, W. Li, Z. Wang, J. Yang, Y. Xiong, D. He, L. Chen, S. Mu, J. Mater. Chem. A 6 (2018) 20093–20099.
[22] T. Wang, Z. Kou, S. Mu, J. Liu, D. He, I.S. Amiinu, W. Meng, K. Zhou, Z. Luo, S. Chaemchuen, F. Verpoort, Adv. Funct. Mater. 28 (2018) 1705048.
[23] I.S. Amiinu, Z. Pu, X. Liu, K.A. Owusu, H.G.R. Monestel, F.O. Boakye, H. Zhang, S. Mu, Adv. Funct. Mater. 27 (2017) 1702300.
[24] Z. Wang, H. Jin, T. Meng, K. Liao, W. Meng, J. Yang, D. He, Y. Xiong, S. Mu, Adv. Funct. Mater. 28 (2018) 1802596.
[25] H. Zhang, J. Nai, L. Yu, X.W. Lou, Joule 1 (2017) 77–107.
[26] E. Hu, Y. Feng, J. Nai, D. Zhao, Y. Hu, X.W. Lou, Energy Environ. Sci. 11 (2018) 872–880.
[27] L. Wu, Q. Li, C.H. Wu, H. Zhu, A. Mendoza-Garcia, B. Shen, J. Guo, S. Sun, J. Am. Chem. Soc. 137 (2015) 7071–7074.
[28] T. Liu, Y. Liang, Q. Liu, X. Sun, Y. He, A.M. Asiri, Electrochem. Commun. 60 (2015) 92–96.
[29] B.Y. Xia, Y. Yan, N. Li, H.B. Wu, X.W. Lou, X. Wang, Nat. Energy 1 (2016) 15006.
[30] H. Zhou, D. He, A.I. Saana, J. Yang, Z. Wang, J. Zhang, Q. Liang, S. Yuan, J. Zhu, S. Mu, Nanoscale 10 (2018) 6147–6154.
[31] I.S. Amiinu, X. Liu, Z. Pu, W. Li, Q. Li, J. Zhang, H. Tang, H. Zhang, S. Mu, Adv. Funct. Mater. 28 (2018) 1704638.
[32] S. Liu, I.S. Amiinu, X. Liu, J. Zhang, M. Bao, T. Meng, S. Mu, Chem. Eng. J. 342 (2018) 163–170.
[33] S. Wang, L. Zhang, Y. Qin, D. Ding, Y. Bu, F. Chu, Y. Kong, M. Liu, J. Power Sources 363 (2017) 260–268.
[34] X.F. Lu, L.F. Gu, J.W. Wang, J.X. Wu, P.Q. Liao, G.R. Li, Adv. Mater. 29 (2017) 1604437.
[35] J. Chen, G. Xia, P. Jiang, Y. Yang, R. Li, R. Shi, J. Su, Q. Chen, ACS Appl. Mater. Interfaces 8 (2016) 13378–13383.
[36] N. Jiang, B. You, M. Sheng, Y. Sun, ChemCatChem 8 (2016) 106–112.
[37] N. Jiang, B. You, M. Sheng, Y. Sun, Angew. Chem. Int. Ed. 54 (2015) 6251–6254.
[38] B. You, N. Jiang, M. Sheng, S. Gul, J. Yano, Y. Sun, Chem. Mater. 27 (2015) 7636–7642.
[39] D. Merki, S. Fierro, H. Vrubel, X. Hu, Chem. Sci. 2 (2011) 1262–1267.
[40] Z. Xing, Q. Liu, A.M. Asiri, X. Sun, Adv. Mater. 26 (2014) 5702–5707.
[41] H. Vrubel, X. Hu, Angew. Chem. Int. Ed. 51 (2012) 12703–12706.
[42] Z. Kou, B. Guo, Y. Zhao, S. Huang, T. Meng, J. Zhang, W. Li, I.S. Amiinu, Z. Pu, M. Wang, M. Jiang, X. Liu, Y. Tang, S. Mu, ACS Appl. Mater. Interfaces 9 (2017) 3702–3712.

[43] Z. Kou, T. Wang, Y. Cai, C. Guan, Z. Pu, C. Zhu, Y. Hu, A.M. Elshahawy, J. Wang, S. Mu, Small Methods 2 (2018) 1700396.
[44] F.X. Ma, H.B. Wu, B.Y. Xia, C.Y. Xu, X.W. Lou, Angew. Chem. Int. Ed. 54 (2015) 15395–15399.
[45] Z. Kou, L. Zhang, Y. Ma, X. Liu, W. Zang, J. Zhang, S. Huang, Y. Du, A.K. Cheetham, J. Wang, Appl. Catal. B Environ. 243 (2019) 678–685.
[46] W. Cui, N. Cheng, Q. Liu, C. Ge, A.M. Asiri, X. Sun, ACS Catal. 4 (2014) 2658–2661.
[47] C. Lu, D. Tranca, J. Zhang, F.N. Rodri Guez Hernandez, Y. Su, X. Zhuang, F. Zhang, G. Seifert, X. Feng, ACS Nano 11 (2017) 3933–3942.
[48] Z. Pu, M. Wang, Z. Kou, I.S. Amiinu, S. Mu, Chem. Commun. 52 (2016) 12753–12756.
[49] P. Yin, T. Yao, Y. Wu, L. Zheng, Y. Lin, W. Liu, H. Ju, J. Zhu, X. Hong, Z. Deng, G. Zhou, S. Wei, Y. Li, Angew. Chem. Int. Ed. 55 (2016) 10800–10805.
[50] M. Fan, H. Chen, Y. Wu, L.-L. Feng, Y. Liu, G.-D. Li, X. Zou, J. Mater. Chem. A 3 (2015) 16320–16326.
[51] S. Wang, A. Morelos-Gómez, Z. Lei, M. Terrones, K. Takeuchi, W. Sugimoto, M. Endo, K. Kaneko, Carbon 96 (2016) 174–183.
[52] Y.N. Hou, Z. Zhao, Z. Yu, Y. Tang, X. Wang, J. Qiu, Chem. Commun. 53 (2017) 7840–7843.
[53] H.B. Wu, B.Y. Xia, L. Yu, X.Y. Yu, X.W. Lou, Nat. Commun. 6 (2015) 6512.
[54] S. Gupta, N. Patel, R. Fernandes, R. Kadrekar, A. Dashora, A.K. Yadav, D. Bhattacharyya, S.N. Jha, A. Miotello, D.C. Kothari, Appl. Catal. B Environ. 192 (2016) 126–133.
[55] K. Xu, H. Cheng, L. Liu, H. Lv, X. Wu, C. Wu, Y. Xie, Nano Lett. 17 (2017) 578–583.
[56] X.L. Tian, L. Wang, B. Chi, Y. Xu, S. Zaman, K. Qi, H. Liu, S. Liao, B.Y. Xia, ACS Catal. 8 (2018) 8970–8975.
[57] J.-Y. Zhang, H. Wang, Y. Tian, Y. Yan, Q. Xue, T. He, H. Liu, C. Wang, Y. Chen, B.Y. Xia, Angew. Chem. Int. Ed. 57 (2018) 7649.
[58] Z.L. Wang, X.F. Hao, Z. Jiang, X.P. Sun, D. Xu, J. Wang, H.X. Zhong, F.L. Meng, X.B. Zhang, J. Am. Chem. Soc. 137 (2015) 15070–15073.
[59] Y. Xue, J. Li, Z. Xue, Y. Li, H. Liu, D. Li, W. Yang, Y. Li, ACS Appl. Mater. Interfaces 8 (2016) 31083–31091.

Qirui Liang received his B.S. degree in 2016 from China University of Mining and Technology in Material Science and Engineering. Currently he is a research master of State Key Laboratory of Advanced Technology for Materials Synthesis and Processing, Wuhan University of Technology. His graduate tutor is Shichun Mu and now his research topic is the application of metal-organic frameworks materials in fuel cell catalysts.

Huihui Jin received her BE and MSc in 2013 and 2015 from Wuhan University of technology. Now she is a PhD student in Wuhan University of technology. Her current research interests lie in the development of non-precious metal for ORR in fuel cell application.

Zhe Wang is a Ph.D candidate at School of Science, Wuhan University of Technology (WUT), China. He received his B.S. and M.S. degree at School of Chemical and Biological Engineering of Changsha University of Science & Technology (2015) and State Key Laboratory of Advanced Technology for Materials Synthesis and Processing in WUT (2018), respectively. His research is mainly focused on graphene-based materials for electromagnetic interference shielding and mechanics.

Dr. Yuli Xiong received her PhD in chemistry from the University of Bath, UK in 2013 and then worked as a postdoc at Huazhong University of Science and Technology, China. Now, she is a lecture in Wuhan Textile University, China. Her research focuses on catalysts and solar cells.

Shuai Yuan received her B.S. degree from the School of Materials Science and Engineering at University of Jinan in 2016. Now she is a master student in fuel cell at Wuhan University of Technology. Her research interests focus on metal-organic frameworks (MOFs) and their applications in electrochemical energy storage.

Xianci Zeng was born in Wuhan, China. She received the Master of Science in Engineering degree in Materials Science & Engineering from University of Pennsylvania in 2018. Currently, she is the research assistant of Prof. Daping He's lab at the Hubei Engineering Research Center of RF-Microwave Technology and Application, Wuhan University of Technology, Wuhan, China. Her research interests include ionic diodes and electrocatalysts for oxygen reduction reaction.

Dr. Daping He is a full professor at Wuhan University of Technology. He obtained his PhD degree in Materials Processing Engineering from Wuhan University of Technology in 2013. He was a Postdoctoral Fellow in the University of Science and Technology of China. Then he joined University of Bath as a Newton International Fellow and University of Cambridge as a Postdoctoral Fellow. His research interest is preparation and application of nano composite materials into new energy devices, sensors and RF microwaves field. He has published over 70 peer-reviewed papers and 5 Chinese patents.

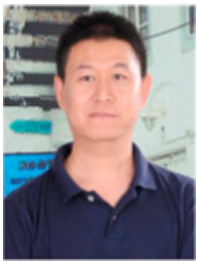

Dr. Shichun Mu is currently working as a professor at Wuhan University of Technology. He received his B.S. degree from Jilin University in 1995 and Ph.D. degree from Chinese Academy of Sciences, China in 2001. Afterwards, he joined the Wuhan University of Technology as a postdoctoral researcher, 2001-2003. He has been a full professor since 2006 at Wuhan University of Technology. He was an academic visitor at Inorganic Chemistry Laboratory, University of Oxford (2007– 2008). His research focuses on nanocarbon materials, PEM fuel cell catalysts, lithium ion battery materials and related devices. He has published over 200 papers and patents.